Published in final edited form as:
Neuroimage. 2010 May 15; 51(1): 135–144. doi:10.1016/j.neuroimage.2009.12.082.

Noninvasive Visualization of Human Dopamine Dynamics from PET Images

E.D. Morris[1,2,3], **C.C. Constantinescu**[4], **J.M. Sullivan**[2,3], **M.D. Normandin**[2,3], and **L.A. Christopher**[5]

[1]Department of Biomedical Engineering, Indiana University-Purdue University at Indianapolis, USA

[2]Department of Biomedical Engineering, Purdue University, W. Lafayette, USA

[3]Department of Radiology, Indiana University School of Medicine, Indianapolis, USA

[4]Department of Psychiatry and Human Behavior, University of California-Irvine, Irvine, USA

[5]Department of Electrical and Computer Engineering, Indiana University-Purdue University at Indianapolis, USA

Abstract

We recently introduced strategies for extracting temporal patterns of brain dopamine fluctuations from dynamic positron emission tomography (PET) data using the tracer, [11C]-raclopride. Each of our methods yields a collection of time-concentration curves for endogenous dopamine. Given a spatially dense collection of curves (i.e., one at every voxel in a region of interest), we produce image volumes of dopamine (DA) concentration, DA($\underline{X}$, t), at multiple voxel locations and each time-frame. The volume over time-frames constitutes a 4D dataset that can be thought of as a DA "movie". There are a number of ways to visualize such data. Viewing cine loops of a slice through the DA volume is one way. Creating images of dopamine peak-time, $T_{peak}(\underline{X})$, derived from a movie, is another. Each visualization may reveal spatio-temporal patterns of neurotransmitter activity heretofore unobservable. We conducted an initial validation experiment in which identical DA responses were induced by an identical task, initiated at different times by the same subject, in two separate PET scans. A comparison of the resulting $T_{peak}(\underline{X})$ images revealed a large contiguous cluster of striatal voxels, on each side, whose DA timing was consistent with the relative timing of the tasks. Hence, the DA movies and their respective peak-time images were shown to be new types of functional image that contain bonafide timing information about a neurotransmitter's response to a stimulus.

Introduction

We have previously introduced different mathematical strategies for extracting temporal patterns of brain dopamine (DA) fluctuations from dynamic PET data using the tracer, [11C]-raclopride (Constantinescu et al., 2007; Constantinescu et al., 2008; Morris et al.,

Corresponding author: E Morris, Yale PET Center, P.O. Box 208048, New Haven, CT 06520, 317 450 6409, evandmorris@gmail.com, evan.morris@yale.edu.
Current address for E. Morris, J. Sullivan, & M. Normandin, Yale PET Center, P.O. Box 208048, New Haven, CT 06520

2005; Morris et al., 2008; Normandin and Morris, 2008; Normandin et al., 2009). Basically, our strategies fall into two general categories: (1) a model of competition between endogenous DA and an exogenous tracer at the post-synaptic D2 receptor site (Morris et al., 2005; Morris et al., 2008; Normandin and Morris, 2008; Normandin et al., 2009), and (2) a decomposition technique, requiring no *a priori* model, to find the additive components (in a linear-algebra sense) of the dynamic PET data that are exclusively related to DA fluctuations (Constantinescu et al., 2007; Constantinescu et al., 2008). Collectively, we call our techniques "ntPET" (for "neurotransmitter PET").

We have begun the process of validating each of our methods. The non-parametric approach (referred to as np-ntPET) was preliminarily applied to PET images of human subjects receiving iv alcohol during the PET scans (Constantinescu et al., 2008). In that analysis, we were able to demonstrate that key characteristics of our regional estimates of (striatal) DA level over time were consistent with our model-based intuition about interactions between neurotransmitters and tracers (Endres and Carson, 1998; Morris and Yoder, 2007; Yoder et al., 2004). For example, subjects whose [11C]-raclopride binding was most affected by alcohol-induced dopamine release had earlier peaking dopamine responses (as predicted by np-ntPET) compared to those who showed lesser change in tracer binding. The parametric models ("p-ntPET") were initially conceived (Fisher et al., 1995; Morris et al., 1995) as extensions of the standard 2-tissue compartment model (Mintun et al., 1984) that is commonly used to model data acquired with receptor-ligand tracers. The p-ntPET model was tested (retrospectively) against microdialysis and shown to predict temporal DA curves that agree nicely with intracerebral microdialysis traces of DA concentration (Morris et al., 2008). One disadvantage of our original parametric approach is its complexity; p-ntPET contains 11 unknown parameters, requiring computationally demanding nonlinear least squares estimation. To address this disadvantage, we introduced linearized versions of the p-ntPET model (Normandin et al., 2009) which have fewer parameters and can be solved rapidly. In doing so, the model-based approach is converging with the nonparametric technique for ease of use. At least as applied to DA, neither approach would require arterial sampling; as linear methods, the computational load for both is minimal and voxel-by-voxel applications of either approach become feasible. The result is that we now have multiple tools to produce time-courses of DA concentration at every voxel in a human brain image (at least in DA-ergic areas) in response to a pharmacological or cognitive perturbation. The data produced by these tools are 4-dimensional which we can represent as DA($\underline{X}$, t), where $\underline{X}$ = x, y, z. (i.e., DA intensity that varies in x, y, z and time). A difficulty posed by the creation of any multidimensional data is that of effective visualization. One natural way to display temporal changes at multiple, high-resolution locations is as a "movie" but visualizing the entire data set over time would require a special 3D display. Practically, we can view a movie (a cine loop in imaging parlance) of a selected 2D slice of the data over time. An alternative way to visualize the data is to select one aspect of the DA curve at each voxel that best represents the temporal behavior of the neurotransmitter and display these voxel values as a new type of parametric image (e.g., an image of the time of peak DA concentration, $T_{peak}(\underline{X})$). Here, we demonstrate both methods for visualizing the temporal behavior of DA. To test the utility of our methods, we apply our new visualizations to the DA responses of a human subject exposed to multiple presentations of an identical test stimulus designed to provoke a consistent and (temporally) predictable release of DA.

PET studies with receptor-ligand-tracers are commonly used to detect changes in endogenous neurotransmitter concentration but conventional methods of analysis (e.g., volumes of distribution, binding potential, occupancy) yield measures that represent *average values* spanning the entire imaging study. Timing information is not preserved; in fact, timing of the neurotransmitter response can be a significant confound to a consistent measurement of magnitude thereof (Yoder et al., 2004). The development of minimally-

invasive imaging assays that could capture the *temporal signatures* of neurotransmitter changes in response to rewarding stimuli represents the possibility of a suite of new research tools for the study of diseases which may cause – or be caused by – disruption of the normal timing of neurotransmitter release. It has been suggested that the development of dyskinesias in some Parkinson's patients may be related to abrupt DA fluctuations following levodopa administration (de la Fuente-Fernandez et al., 2004). Drug abuse may also involve temporal dysregulation of DA. We have been motivated in our work by the hypothesis of Volkow and Swanson (Volkow and Swanson, 2003) that the addictive liability of stimulant drugs is related to their differential effects on dopamine (DA) kinetics in the brain. While there is good supporting evidence for this hypothesis, it cannot yet be tested *directly* in people. Because there is no convenient tracer of endogenous DA that can be used to follow its action on a minute-to-minute basis, we believe the techniques for visualizing DA kinetics presented herein may prove valuable for characterization and visualization of the brain's dopaminergic response to drugs of abuse or therapeutic drugs, or other stimuli and evoked behaviors.

To test our ability to visualize DA changes and quantify their timing, we performed 3 PET scans with [11C]-raclopride on a normal volunteer. As prescribed by our previously developed ntPET methods (Constantinescu et al., 2007; Constantinescu et al., 2008; Morris et al., 2005; Morris et al., 2008; Normandin and Morris, 2008; Normandin et al., 2009), each scan began with a bolus injection of the tracer. One of the scans involved no task or other activation paradigm. What differed between the two remaining ("activation") scans was the *timing* of a motor task, performed by the subject for a consistent duration. The task is known to cause release of striatal DA coincident roughly with its commencement (Alpert et al., 2003; Badgaiyan et al., 2003). Below, we present novel "movies" of DA fluctuations due to task execution and equally novel parametric images of the timing and the *difference* in timing of DA events related to performance of early vs. late motor activity.

Materials and methods

Experimental Protocol

We utilized a motor task intended to cause a robust release of DA in the caudate and putamen at a consistent delay following initiation. The task was based on one used previously by Badgaiyan and colleagues (Alpert et al., 2003; Badgaiyan et al., 2003) that required a subject to repeatedly oppose his right thumb to one of the other fingers of his hand in response to changing visual cues (Fig. 1A). Based on (Alpert et al., 2003; Badgaiyan et al., 2003), it appears that an unrewarded finger-opposition task yields a near-immediate and detectable release of DA.

A right-handed male was scanned after a bolus injection of [11C]raclopride at time 0. Images were acquired by Siemens HR+ scanner in 3D mode. After Fourier rebinning of data, images were reconstructed with filtered back-projection and post-filtered by a 5 mm Gaussian filter. Three 60-minute scans were performed (one "rest"; and two "activation" conditions). A visual prompt (Fig. 1A.) cued a finger-opposition sequence for 10 minutes beginning at a predetermined time. The subject was not told ahead of time when the task would commence. The "early" task lasted from 25 to 35 min; the "late" task occurred from 40 to 50 minutes in a *separate* scan session. PET sessions were separated by at least 2 hours. The inter-cue interval was randomized [0.5 to 2 seconds]. Prior to being scanned, the subject signed an informed consent statement agreeing to participate in the study, which was approved by the Indiana University Institutional Review Board.

Image acquisition and processing

Images were acquired by Siemens ECAT EXACT HR+ scanner in 3D mode. Acquisition began with injection of 15.1 ± 1.4 mCi [11C]raclopride. The specific activity at the time of injection was 3.95 ± 1.1 Ci/umol. After Fourier rebinning of data, images were reconstructed with filtered back-projection and post-filtered by a 5 mm Gaussian filter. Images were initially collected in timeframes of 30 sec for the first 5 minutes and 1 minute frames thereafter for the remaining 55 minutes. Early PET frames were combined to yield equal-length (1 minute) frames throughout the duration of the scan, which was necessary for np-ntPET processing (see below). PET images were corrected for motion and aligned to the subject's structural MRI. The MRI was aligned to Montreal Neurologic Institute (MNI) space and the PET was subsequently aligned to MNI space using the transformation between the subject's MR and MNI space (Tzourio-Mazoyer et al., 2002). Image alignment occurred prior to ntPET processing or visualization.

Nonparametric ntPET

We used the np-ntPET method to analyze the scans acquired for this study (Constantinescu et al., 2007). In brief, singular value decomposition (SVD) was applied to the dynamic PET signals from voxels of interest (the striatum) to define a subspace spanning the rest condition. Mathematically, the decomposition is expressed as,

$$R=U_R \cdot S_R \cdot V_R^T \quad (1)$$

where R is the matrix of rest signals. The resulting singular vectors, or temporal components, are contained in the columns of the matrix U_R. The most significant temporal components corresponding to the K largest singular values (diagonal values of the S_R matrix) were retained in $U^{(K)}$.

The contribution of rest signals to the activated state was "subtracted" from the PET time activity curves (TACs) from the activated condition by subtracting the projection of the "task" signals onto the rest subspace. The projection and subtraction are combined as,

$$B=(I - U_R^{(K)} U_R^{(K)^T}) \cdot A \quad (2)$$

where A is the matrix of signals (TACs) from the activation condition and B are the resulting components related solely to activation. A second SVD was applied to the result of the projection operation, and the most significant components corresponding to the L largest singular values were retained. In earlier simulations of [11C]raclopride scans with multiple overlapping dopaminergic tasks performed during the scan, we showed that the response to each task precipitates an additional -and distinct- temporal component in the PET data that is unique to the activation space. The components can also be identified and retained by the analysis (see figures 3-6 of Constantinescu et al., 2007). The retained components (in the matrix are $B^{(L)}$) are related to the integral of the DA curve. Thus, differentiation of the columns of $B^{(L)}$ with respect to time (and a sign change) yields the desired DA curves. This operation is accomplished with a filter, as shown as follows,

$$\overline{DA}(t) \approx -\frac{dB^{(L)}}{dt} = B^{(L)}(t) \otimes \widehat{\theta} \quad (3)$$

where $\overline{DA}(t)$ are the estimated DA curves. Because the filter operation is similar to a derivative, the scale of B is lost so $\overline{DA}(t)$ represents the deviation from baseline rather than absolute level. A minimum mean square error (MMSE) filter was trained on simulated data to relate PET TACs to the simulated DA curves ("signatures") that were used in creating the

simulations. Filter training (finding filter parameters, $\hat{\theta}$, that map the activation signals, $B^{(L)}$ to the dopamine curves, $\overline{DA}(t)$) was performed using 1000 sets of data consisting of 10 noisy rest signals and 10 noisy task signals. These signals were created using a model of [11C]raclopride uptake in the presence of time-varying dopamine (introduced in Morris et al, 1995) with a wide range of raclopride parameters and dopamine curves. The details are given in Constantinescu et al, 2007. The filter was applied to the significant difference signals to yield DA curves due to task, at each voxel, da(i,j,k, t). (Lower case "da" refers to a single voxel, in this case, located at x=i, y=j, z=k, and whose value varies over time, t.) The important thing about each step in the np-ntPET method, as suggested by equations 1-3 is that they are linear operations and can be performed rapidly at every voxel. Please see (Constantinescu et al., 2007) for details.

Creating DA Movies

DA curves at each voxel, DA($\underline{X}$, t), were produced for every striatal voxel. A single time frame for a DA movie consists of DA($\underline{X}$, t_i) at time, t_i for a fixed z (i.e., a 2D slice of DA values over time). Some areas of the striatum may contain more DA than others in absolute terms. Because we are primarily interested in *temporal* patterns, we normalized the DA intensity at each voxel by the maximum level achieved at that particular voxel. The normalized DA intensity is displayed in color; the color table is included in each movie frame. The frames were collected into a single Audio Video Interleave (*.avi) format that can be displayed in any player that handles that standard. Fig. 1B depicts the progression from PET data to DA movies. Because of unavoidable artifacts that are introduced into the results at the early and late ends of the data (explained in Constantinescu et al., 2007), the movies are truncated to correspond to the time-period from 5 to 55 minutes of the scan.

Creating DA Peak-Time Images

Each individual voxel's DA signal, da(i,j,k, t), was convolved with a 10-min square kernel to facilitate idenfification of the peak time (Constantinescu et al., 2008). The reported $T_{peak}(\underline{X})$ is equal to the peak time of the convolved (smoothed) signal. The width of the kernel was chosen to be consistent with the MMSE filter width (originally applied to each activation signal to extract a DA signal, see Eqn 3). The MMSE filter was 10 min wide (i.e., every 10 adjacent time-points in the B signal were used to estimate each time-point in the DA signal) so it seemed logical to define the peak DA value in terms of 10 minute windows (kernels). Each $t_{peak}(i,j,k)$ (minutes) was assigned to its voxel location to produce DA peak time images, $T_{peak}(\underline{X})$. (Lower case t_{peak} refers to an individual voxel.) Because [11C]-raclopride binding outside the striatum has low contrast, the only voxels that were processed resided in a pre-defined striatal region (Brett et al., 2002) (http://marsbar.sourceforge.net/).

Masking the DA Movies and Peak Time Images

We sought to display the temporal behavior solely of voxels with robust DA release in response to a stimulus. Accordingly, each DA($\underline{X}$, t) data set was masked to include only voxels whose decrease in binding potential (BP_{ND}) (Innis et al., 2007), from rest to activation condition, was greater than or equal to 10%. Although change in BP_{ND} from one scan to another does not convey temporal information about events during the scan, it is commonly used as an average measure of tracer binding. Average change in BP_{ND} from one condition to another is commonly used to indicate tracer displacement due to increased levels of neurotransmitter. The 10% threshold was chosen to exceed published values of test-retest variability in change in BPND for [11C]-raclopride or its SPECT analog (Wang et al., 1999; Kegeles et al., 1999). Masking selected voxels with robust DA-ergic responses. It did not bias our subsequent extraction of temporal information.

Time-Difference Images

Images of the difference in peak times ($\Delta T_{peak}(\underline{X})$, in minutes) were created via a simple algebraic subtraction of the $T_{peak}(\underline{X})$ due to the early task from the $T_{peak}(\underline{X})$ due to the late, voxel-by-voxel.

Segmentation of Peak-Time Difference Images

We assumed that local contiguous clusters of voxels exist that represent brain areas that work in unison to perform a task. If each sub-part of the cluster is activated consistently by a given task (i.e., the sub-part's response is time-invariant relative to the stimulus), then $\Delta T_{peak}(\underline{X})$ for the cluster, made from the two activation conditions above, must include a *single* true value that is equal to the lag between early and late tasks within their respective scan session. Any *variation* around the single true value is assumed to be due to noise inherent in image acquisition and processing. A clustering algorithm was used to identify the clusters of voxels with uniform $\Delta T_{peak}(\underline{X})$. The Bayesian segmentation algorithm that we employed (Christopher et al., 2002; Christopher and Delp, submitted) assumes that the histogram of intensities (delta time values) of the data can be described by a Gaussian mixture model (GMM). The iterative Expectation-Maximization/Minimization of Posterior Marginals (EM/MPM) process by which the ($\Delta T_{peak}(\underline{X})$) images are clustered assumes a neighborhood of voxels in a Markov random field, according to the 6 spatial nearest neighbors in the Bayesian prior distribution function p(x). The degree of regularization (see Eqn. 4, below) determines the likelihood that the process will combine neighboring voxels of similar statistics into a single cluster. The statistics of the whole volume are optimized over the best global fit for the choices of individual voxel classifications. This optimum is reached by maximizing the Bayesian posterior distribution p(x|y), according to:

$$argmax\left\{-\log\sigma_{x_s}-\frac{(y_s-\mu_{x_s})^2}{2\sigma_{x_s}^{\ 2}}-\sum_{\{r,s\}\in C}\beta\, t(x_r,x_s)\right\}$$
$$t(x_r,x_s)-\begin{pmatrix}0;x_r=x_s\\1;x_r\neq x_s\end{pmatrix}\qquad C-\text{clique of } X \tag{4}$$

In the equation above, C defines the 6 voxel neighborhood; x_s is the current classification of a particular voxel at location s corresponding to the unclassified input voxel y_s; x_r are the voxels in C; σ and μ are the parameters of the Gaussian model; β is the regularization parameter (weighting factor for amount of spatial interaction). (The use of X in Eqn. 4 is not related to the naming of the matrix, $\underline{X}$, in Eqns. 1-3.) More details on the clustering algorithm can be found in (Christopher et al., 2002; Christopher and Delp, submitted). We always started with a large number (15) of classes (or Gaussian distributions) whose mean values ranged from -90 to +110 minutes. The algorithm combined classes until convergence was reached. Neither the final number of clusters, nor Gaussian mean values or variances were pre-selected.

Results

Fig. 2A shows part of a dynamic PET data set ("one slice" through the striatum over time). Images from the other two dynamic scans of this subject (one "rest", the other with the motor task initiated at a different time) are indistinguishable, visually, from Fig. 2A. The time-activity data in Fig. 2B correspond to activity of the radiotracer, [11C]-raclopide (nCi/ml) in the right striatum. The TAC shows the typical rapid influx of raclopride and slower efflux from the tissue. An abrupt drop and subsequent recovery of activity appears at or near the time of task performance (25-35 minutes). This "notch" in the TAC contains information about variation in endogenous DA.

Fig. 3 displays representative 1-minute frames of two "DA movies" for the same axial slice through the brain as Fig. 2 (i.e., DA($\underline{X}$,t) for the same, fixed z location). Each voxel in Fig. 3 is scaled to its own maximum; color indicates fraction of maximal DA level achieved at a given time. Fig. 3A is the DA movie for the task initiated early in the scan; Fig. 3B is for the late task. Note the large number of voxels bilaterally, in Fig. 3A whose DA levels are maximal at 26 minutes (just after start of the early task). Fig. 3B, by contrast, shows the DA movie frames for the same subject performing the same task but later (see Methods, Fig. 1A). In this case, maximal DA levels in the striatum appear much later (coincident with late task performance, between 40-50 min.) These data are available for viewing as movies (in *.avi format) as supplemental Videos 1 and 2.

Dopamine Peak-Time Images

The frames of the DA movies are illustrative of the minute-to-minute fluctuations of endogenous DA level in response to a task. The time-varying patterns in Fig. 3 have not previously been observed or – perhaps – imagined. While the DA movies suggest a tight correspondence between motor activation and maximal DA release, we sought additional confirmation of our impressions of these newly-created image sequences. To reduce the 4D DA movies into a more manageable 3D format, we created a new parametric image of DA kinetics: the DA peak-time image, $T_{peak}(\underline{X})$. The $T_{peak}(\underline{X})$ images convey some of the temporal information of the movies but in a quantitative and journal-friendly format. Fig. 4A shows $T_{peak}(\underline{X})$ corresponding to the DA($\underline{X}$, t) in Fig. 3A. The units of the peak-time image (which are displayed in color) are minutes. An annotated color bar is shown at the right. A large area of blue, bilaterally, indicates that the peak DA activity occurs at or around 26 minutes into the scan session (with task start at 25 minutes and duration 10 minutes). The histogram of all striatal voxel values in the slice confirms the behavior. The histogram contains two subpopulations of voxels that peak at slightly different times during task performance. A third peak of very-late peaking voxels is also present. Fig. 4B shows the comparable $T_{peak}(\underline{X})$ image for a scan session containing the identical task starting at 40 minutes. The overwhelming majority of voxels in the latter image peak between 43 and 52 minutes as can be seen in the image and, respectively, in the histogram. The histogram in Fig. 4B also suggests a bifurcation of the kinetic behavior of the voxels that peak during the task into (at least) two sub-classes.

Time-Difference Images

As an additional test of the validity of the temporal information in our DA movies and peak time images, we posed the question: if two dopaminergic tasks are identical in every way except the timing of when they start, shouldn't the *difference* in their DA peak time images faithfully reflect this temporal difference? The voxel-by-voxel image of difference in DA peak time, $\Delta T_{peak}(\underline{X})$, is displayed in Fig. 5A for the anatomical slice in Figs. 2 - 4. Most of the voxel values in the difference map shown (calculated as late $T_{peak}(\underline{X})$ − early $T_{peak}(\underline{X})$) range from 10-25 minutes. The histogram below Fig. 5A is for the *whole striatal volume* (not just one slice). While it confirms that the voxel values are mostly positive differences (i.e., late $T_{peak}(\underline{X})$ reflects DA events that occurred *later* in a scan than the early $T_{peak}(\underline{X})$) the histogram takes no account of the spatial arrangement of temporally similar voxels.

Cluster of Synchronized Dopamine Activity

To probe the spatial cohesion of striatal areas that are temporally related to the task, we applied a clustering algorithm as described briefly, above (Christopher et al., 2002; Christopher and Delp, submitted). The clustered version of Fig. 5A is shown in Fig. 5B. (The histogram in Fig. 5B is for the entire striatal volume, post-clustering.) Iterative segmentation yielded 6 distinct classes of voxels. The dominant class, containing 1883 (1 mm^3) voxels had a mean (difference) value of 17.48 +/- 11.78 (mean +/- sd) minutes. This

largest cluster of voxels (62.35% of all the activated voxels) appears to be temporally consistent with the relative timing of the early and late tasks because its difference value (17.48 min.) is very nearly equal to the time-lag between tasks (15 min.) It is rendered in Fig. 6. The cluster (viewed from the posterior aspect of the brain) includes roughly equal numbers of voxels, bilaterally.

Discussion

Case for Temporal Information in DA movies and Peak Time Images

DA fluctuations in humans, in vivo, have not been measured previously (save for a few studies using microdialysis in pre-surgical patients (e.g., (Fried et al., 2001)). We believe that ntPET (Constantinescu et al., 2007; Constantinescu et al., 2008; Morris et al., 2005; Morris et al., 2008; Normandin and Morris, 2008; Normandin et al., 2009) provides the means to make such measurements but it is difficult to know what to expect of the results. The absence of a gold-standard forced us to design an experiment for which the DA response was predictable. We chose a finger opposition task. But because the task was performed over 10 minutes, it was reasonable that we would find a distribution of responses (see histograms in Figs. 4A and 4B.) To verify that these responses were reflective of DA timing information, we calculated the *difference* between peak times for late and early task performances on a voxel-by-voxel basis (Fig. 5A). We reasoned that whatever the timing of the DA response within a given voxel relative to task performance, such timing should be invariant across multiple performances of the same task. Thus, if $\Delta T_{peak}(\underline{X})$ contains a substantial grouping of voxels whose value is nearly equal to the experimental delay between tasks, this group (class) of voxels must be associated with the task. An iterative clustering algorithm was used to refine the $\Delta T_{peak}(\underline{X})$ image (Fig. 5B) and to more clearly identify the class of voxels we sought. We found that the largest class of voxels behaved nearly as predicted. This finding is thus supportive of our new modeling/image processing techniques. ntPET generates new (image) data types that may be useful in neuroscience research studies or even in clinical practice in which timing of neurotransmitter response is at issue.

Possible Uses for DA Movies and Peak Time Images

We have introduced two new types of functional images derived from dynamic PET data. The first type, DA($\underline{X}$, t), can be thought of as a movie of fractional DA level over time during the course of a PET session. Like most dynamic medical image data, this is a 4D data set but individual slices can be viewed over time to provide qualitative temporal information. Such movies of the DA system at work may reveal spatio-temporal patterns of activity not previously observed in living subjects, and certainly not in humans. As visualization techniques advance, one could imagine a movie made from a series of 3D rendered images (ala Fig. 6) which would give even more complete view of the progressive involvement of brain regions over time. The new images of DA activity presented herein would not have been possible without our prior theoretical work to develop ntPET that maps tracer uptake and displacement to changing DA levels.

A second new image type is DA peak-time, $T_{peak}(\underline{X})$. This image may prove most useful to researchers because, as diagrammed in Fig. 1, it reduces the dimensionality of the temporal information in DA($\underline{X}$, t) to a single 3D data volume. One way to use $T_{peak}(\underline{X})$ is to calculate a simple difference between two of them. The $\Delta T_{peak}(\underline{X})$ image in Fig. 5 shows (particularly after clustering) that a large, contiguous cluster of voxels exists whose DA timing is roughly consistent with the performance of a DA-ergic task. The cluster does not encompass the whole striatum nor is it perfectly symmetric. At this point, we are not interested in the exact anatomical extent of the cluster because this study was merely an exploration/demonstration

of the analysis procedure. However, the prospective ability to detect regions whose DA-ergic response pattern changes with age or drug could illuminate progression of disease or response to therapy. The concept of a DA peak-time is similar to the common concept in pharmacology of T_{max}, the time at which a drug reaches its maximum level in tissue. It is possible that with the proper modifications, the ntPET methods could be used to produce voxel-by-voxel images of T_{max} for a competitor drug rather than (or in conjunction with) T_{peak} for the endogenous competitor.

There is a tradition in PET research, dating to blood flow studies with [15O]-water, of using the difference between images as a marker of "activation" (e.g., (Fox et al., 1986)). It is conceivable that much of the existing infrastructure of SPM (Friston et al., 1995) or other statistical innovations could be applied to our $\Delta T_{peak}(\underline{X})$ images to probe for significant effects of brain activity mediated by neurotransmitter changes. The observation that the time value of the largest cluster in Fig. 5 agrees well with the spacing in time of the tasks suggests that $T_{peak}(\underline{X})$ and $\Delta T_{peak}(\underline{X})$ are quantitative images. Drugs or learning effects that delay or speed up neurotransmitter action by minutes may now be identifiable, non-invasively.

Given a suitable ligand, ntPET techniques and visualization approaches presented herein should be applicable. There has been much greater success in detecting displacement (via PET) of ligands for DA receptors than for other receptors. Nevertheless, there is a great deal of effort being directed toward the identification of displaceable serotonin ligands (e.g., Finnema et al., 2009). Once serotonin ligands with kinetics comparable to raclopide are developed, the applicability of our methods will be expanded to explore serotonin kinetics.

Alternative Explanations for our Results

1. It is reasonable to seek alternative explanations for the timing difference that we see in Fig. 5 and that we cite as evidence of ntPET utility. If the initiation of the task were to have induced unwanted head motion at comparable moments in both early and late tasks, we might see the type of behavior in the [11C]-raclopride TAC (Fig. 2B). However, all images were motion corrected and aligned to a common orientation using standard techniques. Further, $T_{peak}(\underline{X})$ and histograms in Fig. 4 suggest multiple classes of responses. It seems unlikely that head jerks would be so repeatable – none were observed by the investigators.

2. A much-debated claim in the PET literature calls into question the applicability of a strict competition-based model for displacement of PET tracers. In the presence of DA releasing agents such as amphetamine, it appears that the (short-lived) effect of increased DA concentration alone may not completely explain a prolonged downward deflection of the [11C]-raclopride curve (Houston et al., 2004). If post-synaptic DA receptors bound to DA were to be internalized, they would be less readily available to tracer. However, such observations and their attendant hypotheses are not relevant here. The TAC in Fig. 2B clearly shows that the magnitude of the deflection of [11C]-raclopride curve is mild (internalization has been invoked at high occupancy of DA receptors) and the effect is obviously short-lived.

3. The Bayesian segmentation algorithm applied to Fig. 5A yielding Fig. 5B is an iterative one. It requires an initial guess of distinct classes of voxels, their mean (difference) values, and variances. We segmented the data multiple times with different starting guesses for number of classes and means. Each time, the algorithm converged to a result containing a large class of voxels with mean between 14.6 and 17.4 minutes.

4. The histograms of $T_{peak}(\underline{X})$ in Figs. 4A and 4B suggest that during the course of the task the DA-ergic response may consist of primary and secondary phases. This is an interesting finding which demands further investigation. It is not surprising that the two phases of the response merge into one (dominant) class of voxels in the $\Delta T_{peak}(\underline{X})$ map (Fig. 5). Recall the premise of our experimental design. Whether a class of voxels responds to the initiation of a task or to its persistence, we assume that these classes and their respective behaviors are fixed. Thus, the *difference*, $\Delta t_{peak}(i,j,k)$, for any associated voxel, (i,j,k), will be the same.

5. There are voxels with late $T_{peak}(\underline{X})$ that are not associated with either task. These may be a result of a documented artifact in np-ntPET at the end of the scan session (the reason we truncate the movies at 55 minutes). But if the artifact is consistent, such voxels will have a zero value in $\Delta T_{peak}(\underline{X})$. Similarly, the original presentation of np-ntPET also determined that the variance in peak-time estimates degrades slightly for events that occur later in the scan session (Constantinescu et al., 2007). In practice, the method may be maximally sensitive to events that occur in the early part of the scan and future studies can be designed with these limitations in mind.

Conclusion

We have previously developed new methods for extracting temporal information on changes in an endogenous neurotransmitter from dynamic PET data. Such data are 4-dimensional and demand new methods of visualization. Here, we have explored two approaches to displaying dynamic, voxel-by-voxel, representations of DA level and have applied the approaches to a proof-of-concept experiment. Clustering of the output images can help to identify and validate the information contained therein. The results suggest that DA movies and DA peak-time images of events (responses) that occur on the minute time scale may be possible endpoints of PET studies with a receptor tracer.

Supplementary Material

Refer to Web version on PubMed Central for supplementary material.

Acknowledgments

R21 AA015077 (to EDM), Purdue Ross Fellowship (to JMS), and the Indiana Center for Excellence in Biomedical Imaging.

References

Alpert NM, Badgaiyan RD, Livni E, Fischman AJ. A novel method for noninvabsive detection of neuromodulatory changes in specific neurotransmitter systems. Neuroimage. 2003; 19:1049–1060. [PubMed: 12880831]

Badgaiyan RD, Fischman AJ, Alpert NM. Striatal dopamine release during unrewarded motor task in human volunteers. Neuroreport. 2003; 14:1421–1424. [PubMed: 12960756]

Brett, M.; Anton, JL.; Valabregue, R.; Poline, JB. Region of interest analysis using an SPM toolbox. 8th International Conference on Functional Mapping of the Human Brain; 2002.

Christopher LE, Delp E, Meyer C, Carson P. 3-D Bayesian ultrasound breast image segmentation using the EM-MPM algorithm. Proceedings of the IEEE Symposium on Biomedical Imaging (ISBI). 2002:86–89.

Christopher LE, Delp EJ. A Comparison of Bayesian Segmentation Techniques in 3D Breast Ultrasound Imaging. Submitted.

Constantinescu CC, Bouman C, Morris ED. Nonparametric extraction of transient changes in neurotransmitter concentration from dynamic PET data. IEEE Trans Med Imaging. 2007; 26:359–373. [PubMed: 17354641]

Constantinescu CC, Yoder KK, Kareken DA, Bouman CA, O'Connor SJ, Normandin MD, Morris ED. Estimation from PET data of transient changes in dopamine concentration induced by alcohol: support for a non-parametric signal estimation method. Phys Med Biol. 2008; 53:1353–1367. [PubMed: 18296766]

de la Fuente-Fernandez R, Sossi V, Huang Z, Furtado S, Lu JQ, Calne DB, Ruth TJ, Stoessl AJ. Levodopa-induced changes in synaptic dopamine levels increase with progression of Parkinson's disease: implications for dyskinesias. Brain. 2004; 127:2747–2754. [PubMed: 15329355]

Endres CJ, Carson RE. Assessment of dynamic neurotransmitter changes with bolus or infusion delivery of neuroreceptor ligands. J Cereb Blood Flow Metab. 1998; 18:1196–1210. [PubMed: 9809509]

Finnema SJ, Varrone A, Hwang TJ, Gulyas B, Pierson E, Farde L, Halldin C. Fenfluramine decreases 5-HT1B binding of [11C]AZ10419369 in the primate brain. J Cereb Blood Flow Metab. 29:S66.

Fisher RE, Morris ED, Alpert NM, Fischman AJ. *In vivo* imaging of neuromodulatory synaptic transmission using PET: a review of relevant neurophysiology. Human Brain Mapping. 1995:24–34.

Fox PT, Mintun MA, Raichle ME, Miezin FM, Allman JM, Vanessen DC. Mapping Human Visual-Cortex with Positron Emission Tomography. Nature. 1986; 323:806–809. [PubMed: 3534580]

Fried I, Wilson CL, Morrow JW, Cameron KA, Behnke ED, Ackerson LC, Maidment NT. Increased dopamine release in the human amygdala during performance of cognitive tasks. Nat Neurosci. 2001; 4:201–206. [PubMed: 11175882]

Friston KJ, Holmes AP, Worsley KJ, Pioline JP, Frith CD, Frackowiak RSJ. Statistical parametric maps in functional imaging: a general linear apporach. Human Brain Mapping. 1995; 2:189–210.

Houston GC, Hume SP, Hirani E, Goggi JL, Grasby PM. Temporal characterisation of amphetamine-induced dopamine release assessed with [11C]raclopride in anaesthetised rodents. Synapse. 2004; 51:206–212. [PubMed: 14666518]

Innis RB, Cunningham VJ, Delforge J, Fujita M, Gjedde A, Gunn R, Holden J, Houle S, Huang SC, Ichise M, Iida H, Ito H, Kimura Y, Koeppe RA, Knudsen GM, Knuuti J, Lammertsma AA, Laruelle M, Logan J, Maguire RP, Mintun M, Morris ED, Parsey R, Price JC, Slifstein M, Sossi V, Suhara T, Votaw JR, Wong DF, Carson RE. Consensus nomenclature for in vivo imaging of reversibly-binding radioligands. J Cereb Blood Flow Metab. 2007; 9:1533–9. [PubMed: 17519979]

Kegeles LS, Zea-Ponce Y, Abi-Dargham A, Rodenhiser J, Wang T, Weiss R, Van Heertum RL, Mann JJ, Laruelle M. Stability of [123I]IBZM SPECT measurement of amphetamine-induced striatal dopamine release in humans. Synapse. 1999; 31:302–308. [PubMed: 10051112]

Mintun MA, Raichle ME, Kilbourn MR, Wooten GF, Welch MJ. A quantitative model for the in vivo assessment of drug binding sites with positron emission tomography. Ann Neurol. 1984; 15:217–227. [PubMed: 6609679]

Morris ED, Fisher RE, Alpert NM, Rauch SL, Fischman AJ. In vivo imaging of neuromodulation using positron emission tomography: Optimal ligand characteristics and task length for detection of activation. Human Brain Mapping. 1995:35–55.

Morris ED, Normandin MD, Schiffer WK. Initial comparison of ntPET with microdialysis measurements of methamphetamine-induced dopamine release in rats: Support for estimation of dopamine curves from PET data. Molecular Imaging and Biology. 2008; 10:67–73. [PubMed: 18176804]

Morris ED, Yoder KK. Positron emission tomography displacement sensitivity: predicting binding potential change for positron emission tomography tracers based on their kinetic characteristics. J Cereb Blood Flow Metab. 2007; 27:606–617. [PubMed: 16788713]

Morris ED, Yoder KK, Wang C, Normandin MD, Zheng QH, Mock B, Muzic RF Jr, Froehlich JC. ntPET: a new application of PET imaging for characterizing the kinetics of endogenous neurotransmitter release. Mol Imaging. 2005; 4:473–489. [PubMed: 16285909]

Normandin MD, Badgaiyan RD, Schiffer WK, Morris ED. A linear simplification of the parametric ntPET model for estimation of neurotransmitter response kinetics. J Nucl Med. 2009; 50(Suppl 2): 58.

Normandin MD, Badgayian R, Alpert N, Fischman A, Morris E. A linear model for characterizing neurotransmitter release dynamics from PET data. 48. 2007:160P.

Normandin MD, Morris ED. Estimating neurotransmitter kinetics with ntPET: a simulation study of temporal precision and effects of biased data. Neuroimage. 2008; 39:1162–1179. [PubMed: 18023364]

Tzourio-Mazoyer N, Landeau B, Papathanassiou D, Crivello F, Etard O, Delcroix N, Mazoyer B, Joliot M. Automated anatomical labeling of activations in SPM using a macroscopic anatomical parcellation of the MNI MRI single-subject brain. Neuroimage. 2002; 15:273–289. [PubMed: 11771995]

Volkow ND, Swanson JM. Variables that affect the clinical use and abuse of methylphenidate in the treatment of ADHD. Am J Psychiatry. 2003; 160:1909–1918. [PubMed: 14594733]

Wang GJ, Volkow ND, Fowler JS, Logan J, Pappas NR, Wong CT, Hitzemann RJ, Netusil N. Reproducibility of repeated measures of endogenous dopamine competition with [11C]raclopride in the human brain in response to methylphenidate. J Nucl Med. 1999; 40:1285–1291. [PubMed: 10450679]

Yoder KK, Wang C, Morris ED. Change in binding potential as a quantitative index of neurotransmitter release is highly sensitive to relative timing and kinetics of the tracer and the endogenous ligand. J Nucl Med. 2004; 45:903–911. [PubMed: 15136642]

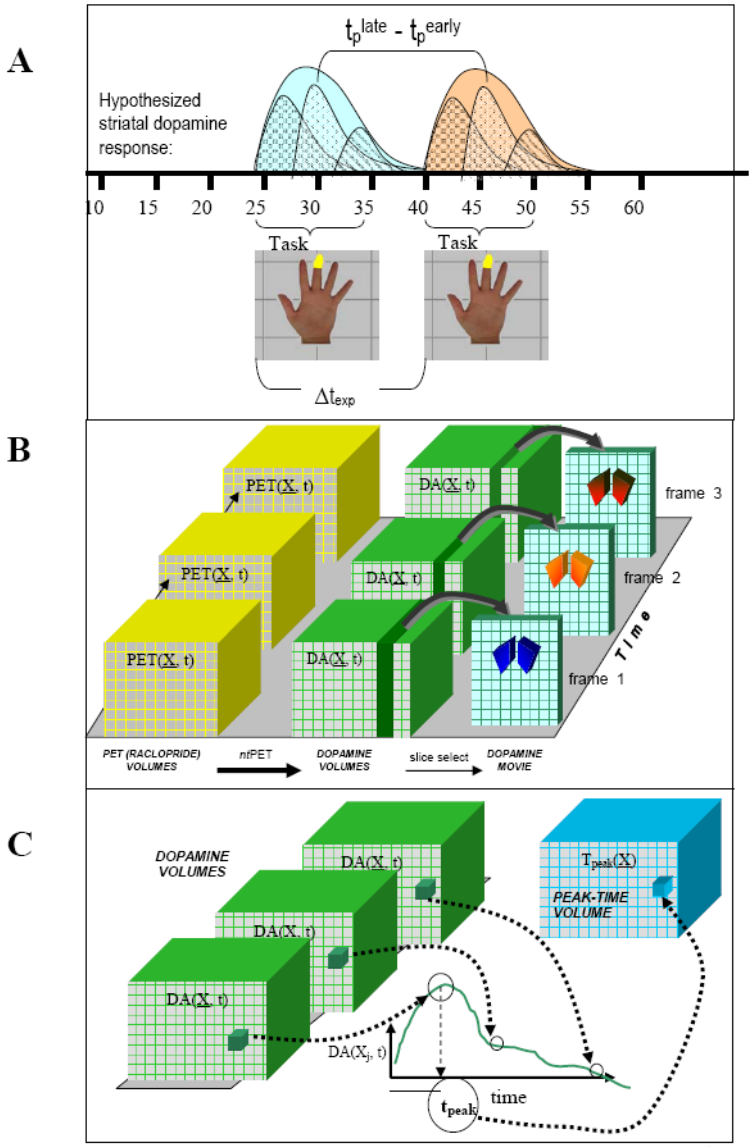

Fig. 1. Methods for visualizing DA dynamics

(A). Timeline for early or late task performance (no more than one task is performed in a given scan session) and expected DA response (above time-line). DA response may be a sum of multiple distinct responses but the absolute time of the task performance should not alter the composition of the response. That is, the experimental delay, Δt_{exp}, between tasks should be reflected in the difference in peak times, $t_p^{late} - t_p^{early}$, for any class of voxels. (B). Given a time-series of PET image volumes, PET(X, t), ntPET analysis (Constantinescu et al., 2007) yields a time-series of DA volumes, DA(X, t). This new time-series can be viewed as a cine loop for a given slice (see for example, Fig. 3). (C). Alternatively, the DA time-series, DA(X, t) can be converted to a parametric image volume $T_{peak}(X, t)$ by extracting the time of peak DA level at each voxel and creating a new data volume with these values (see for example, Fig. 4).

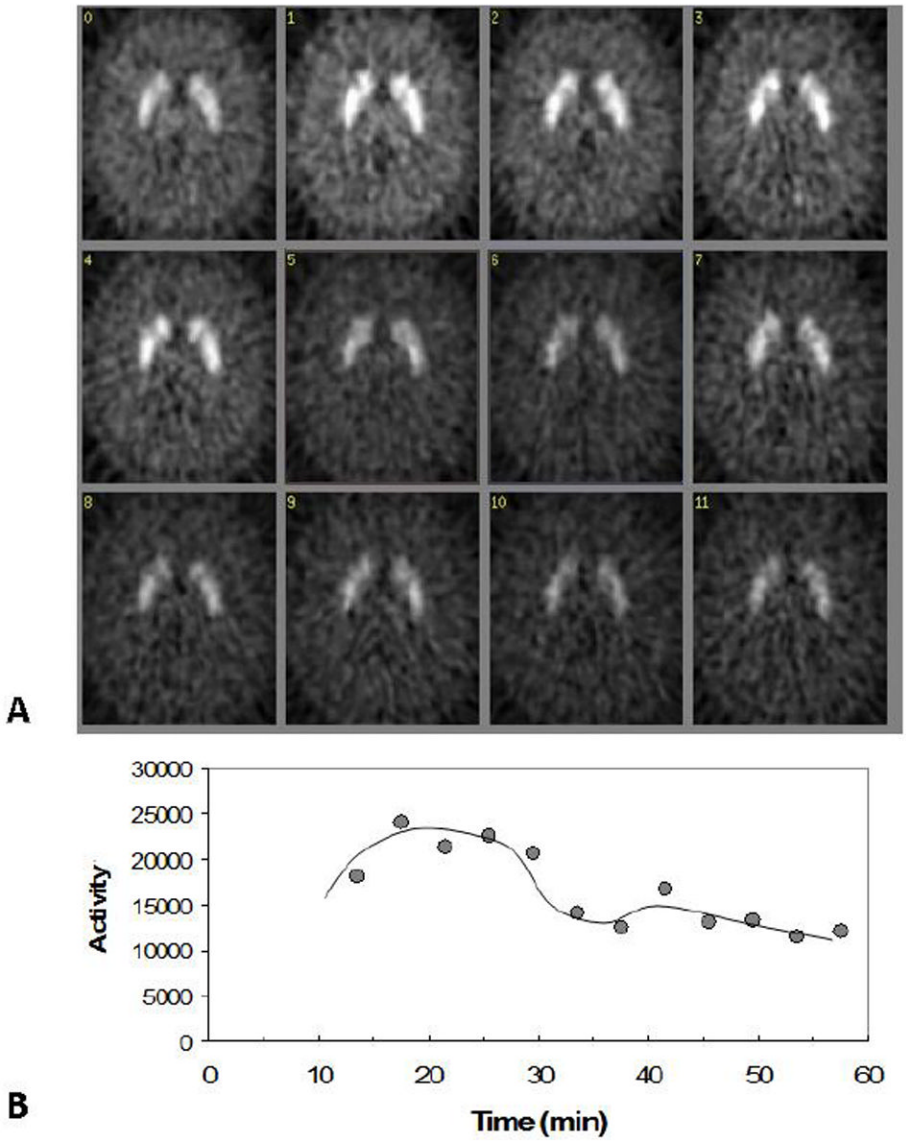

Fig. 2. PET data

(A) [11C]-raclopride images of the subject over time during an "activation" scan session (motor task from 25-35 min). All frames are of a single axial slice through the striatum. White is high and black is low concentration of radioactivity. Frames correspond to 1 minute acquisitions beginning at 13, 17, 21, 25, 29, 33, 37, 41, 45, 49, 53, and 57 minutes, respectively. (Contiguous time frames from 0-60 minutes were acquired and analyzed. We show selected frames merely to simplify the figures.) Images are corrected for radioactive decay. Average values from the right striatum in each frame are plotted in (B). A *hand-drawn* curve suggests an effect of motor task on binding of [11C]-raclopride but a model or other deconvolution technique is needed to extract the precise temporal effect of DA on tracer binding. Note also that after duration of task, [11C]-raclopride concentration appears to return to pre-task trajectory. All images are shown in radiologic convention (left side of brain is on right.)

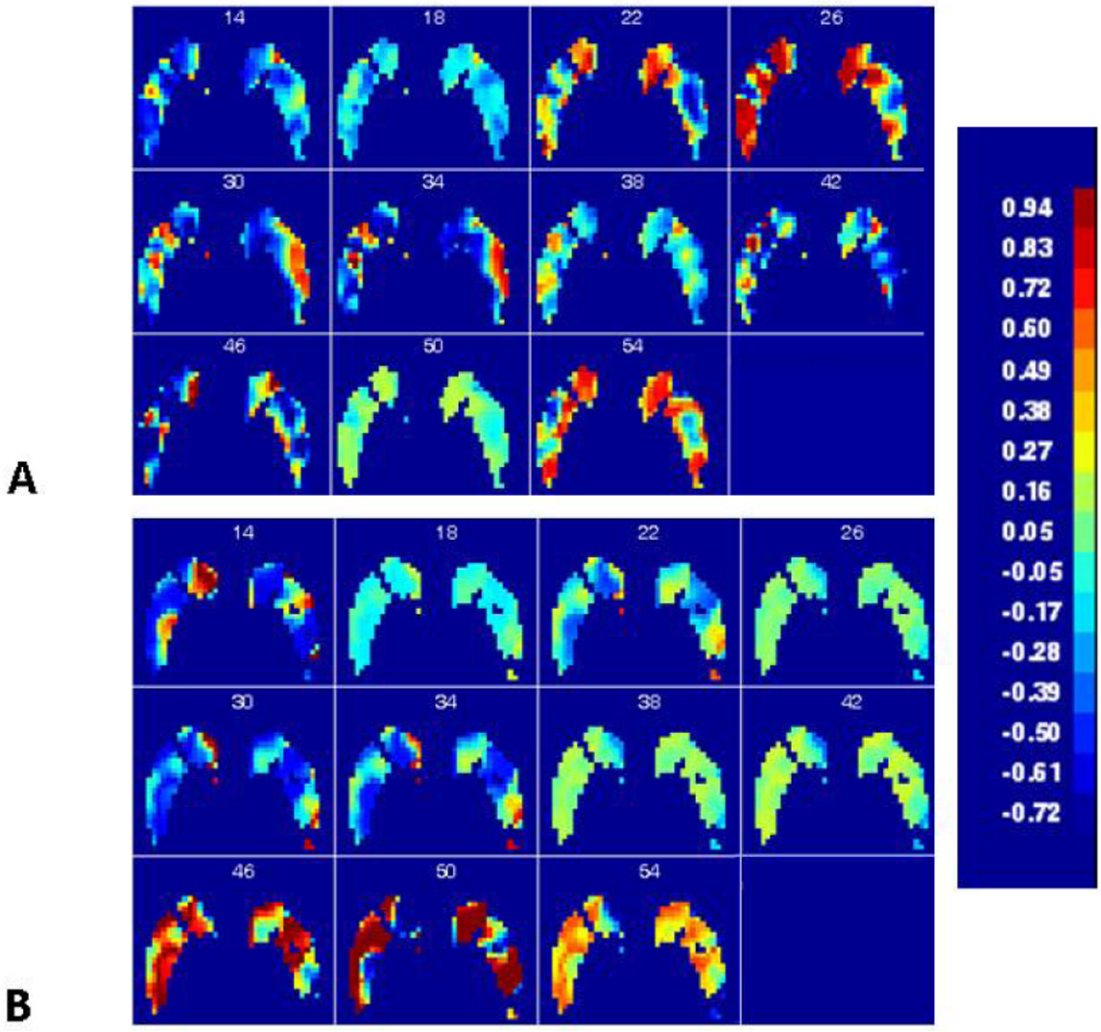

Fig. 3. DA movies, DA(X, t)

(A). One minute frames of a DA movie for early task performance. Color scale represents fraction of maximal DA increase (decrease) above (below) baseline, achieved at each voxel, separately. All frames are of a single axial slice through the striatum (the same slice as in Fig. 2). Every fourth frame was selected for ease of display in this figure; frames are 1 minute long beginning at 14, 18, 22, 26, 30, 34, 38, 42, 46, 50, and 54 minutes after 11C-raclopride injection, respectively. The movies (available as supplemental data) contain contiguous time-frames from 5-55 minutes of the scan. Maximal levels of DA (brownish red) occur in many striatal voxels following initiation of the early task (at 25 min.) (B). Frames of DA movie for late task performance. Frames correspond to the same 1 minute frames selected for display as in (A). Note: high levels of DA (brownish red) occur in many voxels following initiation of the late task (at 40min.) All slices are in axial orientation as in Fig. 2. All images are shown in radiologic convention (left side of brain is on right).

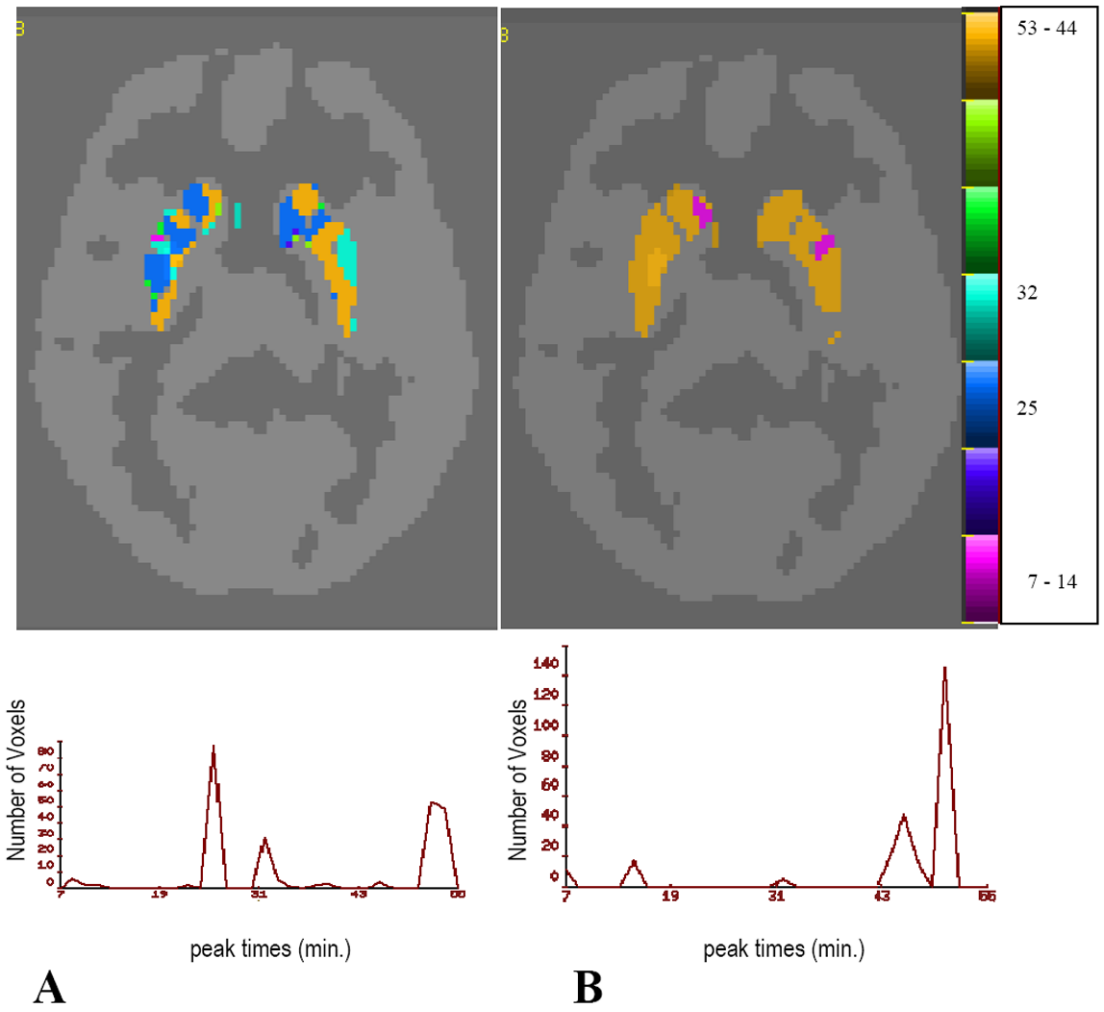

Fig. 4. DA peak-time images, $T_{peak}(\underline{X})$

(A). $T_{peak}(\underline{X})$ for early task (overlaid on mean PET image). Colors indicate peak times in minutes (color bar at right). Histogram below image indicates that most striatal voxels experience peak DA level between 25 and 35 minutes (time of task performance); histogram is for slice shown, only. Slice is same as in other figures. (B). $T_{peak}(\underline{X})$ for late task. Colors indicate peak-times in minutes. The histogram below (for the displayed slice only) indicates that most striatal voxels shown experience peak DA levels between approximately 42 and 52 minutes (task was performed between 40-50 minutes following scan start.) Comparison between histograms clearly shows shift in DA peak-time from early to late. Voxels that peak late in both scans are probably not associated with task performance. Note different scales on histograms.

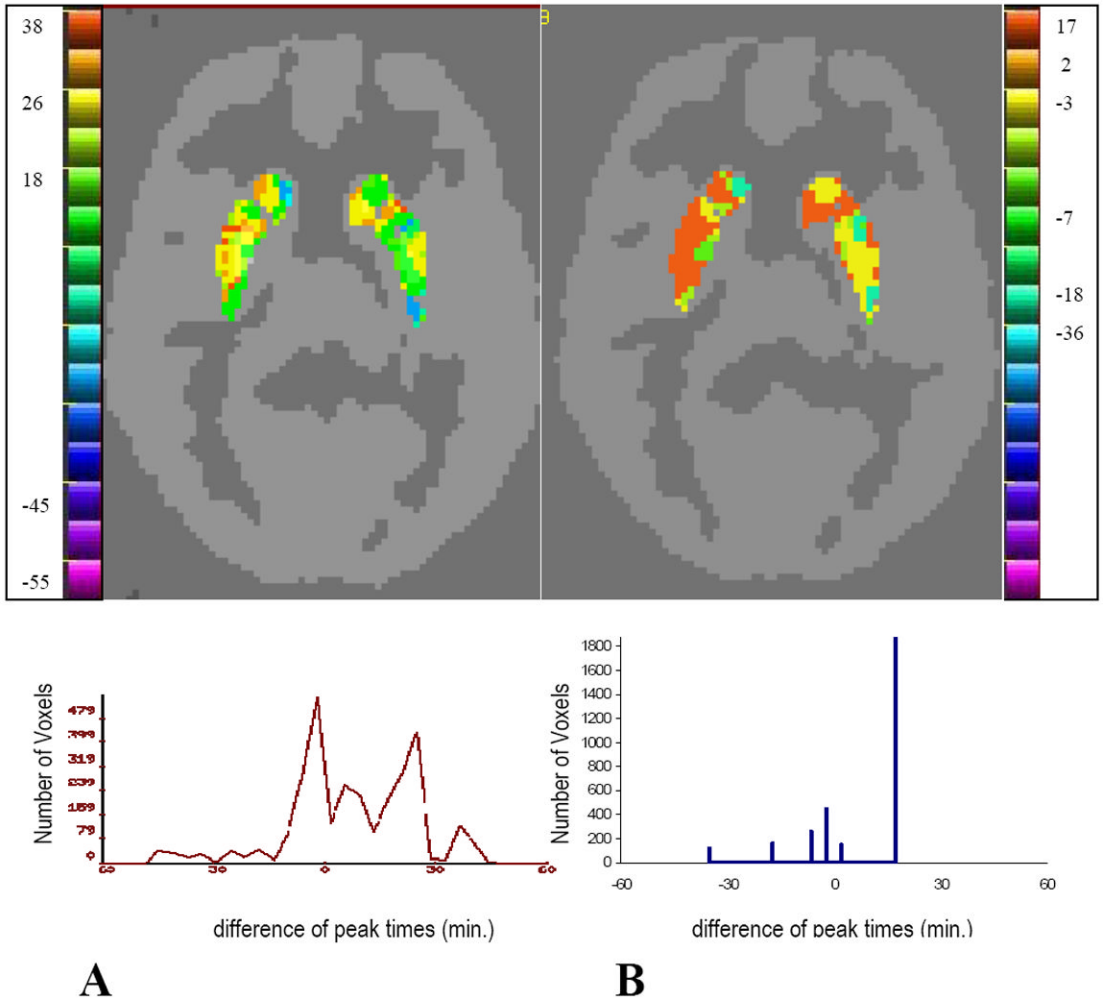

Fig. 5. Difference in peak-time images, $\Delta T_{peak}(\underline{X})$

(A). Difference between late task $T_{peak}(\underline{X})$ (Fig. 4b) and early task $T_{peak}(\underline{X})$ (Fig. 4a). Same slice as in previous figures. Units are in minutes. Color bar on left indicates approximate values of colored striatal voxels. Histogram below image is for *entire volume*, not just displayed slice. Note predominance of positive values for late peak times minus early peak-times. (B). Segmented $\Delta T_{peak}(\underline{X})$. Image in (A) has been segmented according to Bayesian clustering algorithm of Christopher et al. (submitted). Colors correspond to approximate values in color table on right. Not all peak times found in the volume occur on the displayed slice. Histogram beneath segmented image (for entire volume) indicates 6 distinct clusters of voxels with different DA signatures. Dominant cluster has mean DA peak-time value of 17.4 minutes which is in agreement with an experimental time difference of 15 minutes in between onset of early and late tasks. Note different scales on histograms.

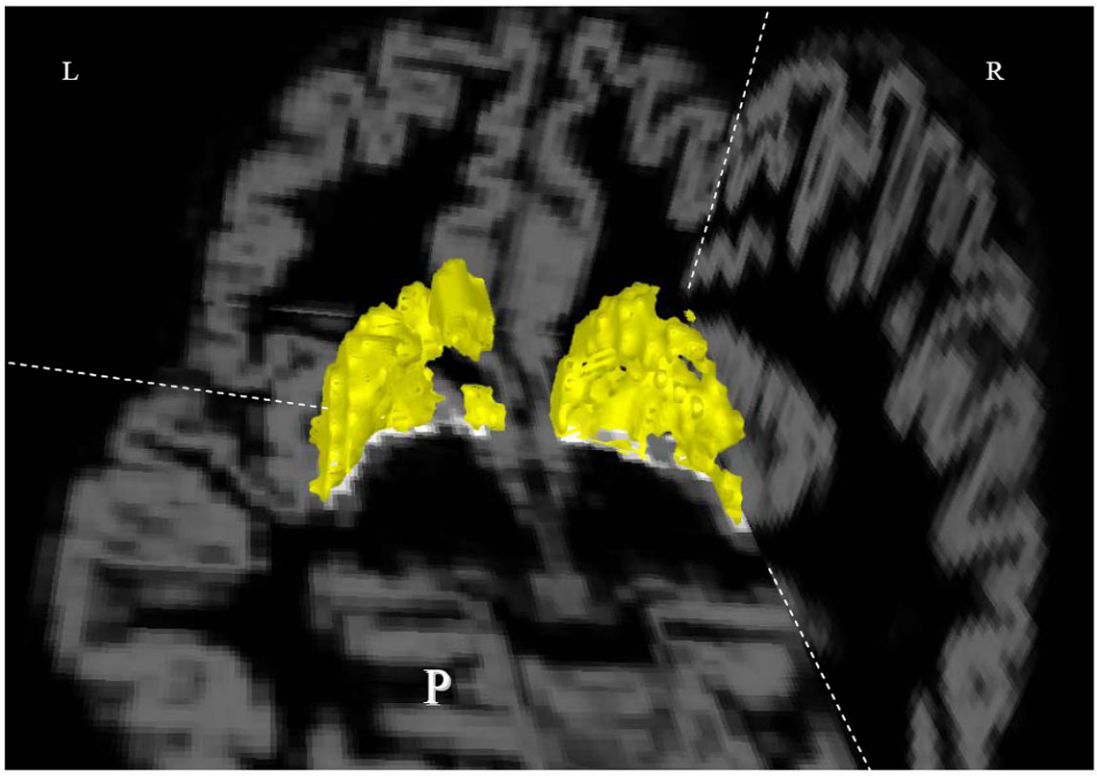

Fig. 6.

Cluster of activated voxels. Three dimensional rendering of the cluster of voxels whose mean difference in DA peak times is 17.4 minutes. These voxels appear to be synched to the motor task performed by the subject. This can be considered a new type of image of a brain region that works in unison, neurochemically, to accomplish a task.